METRICA
METRology Institutional CAtalog

ISTITUTO NAZIONALE DI RICERCA METROLOGICA
Repository Istituzionale

Iridescent Daytime Radiative Cooling with No Absorption Peaks in the Visible Range

This is the author's submitted version of the contribution published as:

Original
Iridescent Daytime Radiative Cooling with No Absorption Peaks in the Visible Range / Ding, Zhenmin; Pattelli, Lorenzo; Xu, Hongbo; Sun, Wenhai; Li, Xin; Pan, Lei; Zhao, Jiupeng; Wang, Chengyu; Zhang, Xiang; Song, Ying; Qiu, Jun; Li, Yao; Yang, Ronggui. - In: SMALL. - ISSN 1613-6810. - (2022), pp. e2202400-1-e2202400-9. [10.1002/smll.202202400]

Availability:
This version is available at: 11696/74459 since: 2022-06-21T15:01:41Z

Publisher:
Wiley

Published
DOI:10.1002/smll.202202400

Terms of use:

This article is made available under terms and conditions as specified in the corresponding bibliographic description in the repository

Publisher copyright
WILEY PRE PRINT
This article may be used for non-commercial purposes in accordance with Wiley Terms and Conditions for Use of Self-Archived Versions.

(Article begins on next page)

18 May 2024

This is the pre-peer reviewed version of the following article: Ding, Z., Pattelli, L., Xu, H., Sun, W., Li, X., Pan, L., Zhao, J., Wang, C., Zhang, X., Song, Y., Qiu, J., Li, Y., Yang, R., Iridescent Daytime Radiative Cooling with No Absorption Peaks in the Visible Range. Small *2022, 2202400, which has been published in final form at https://doi.org/10.1002/smll.202202400. This article may be used for non-commercial purposes in accordance with Wiley Terms and Conditions for Use of Self-Archived Versions.*

Iridescent Daytime Radiative Cooling with no Absorption Peaks in the Visible Range

*Zhenmin Ding, Lorenzo Pattelli, Hongbo Xu *, Wenhai Sun, Xin Li, Lei Pan, Jiupeng Zhao, Chengyu Wang, Xiang Zhang, Ying Song, Jun Qiu, Yao Li *, and Ronggui Yang **

Dr. Z. Ding, Prof. H. Xu, Dr. X. Li, Dr. L. Pan, Prof. J. Zhao, Prof. Y. Song,
School of Chemistry and Chemical Engineering, Harbin Institute of Technology, Harbin, 150001, PR China
E-mail: iamxhb@hit.edu.cn

Dr. L. Pattelli
Istituto Nazionale di Ricerca Metrologica (INRiM), Turin, 10135, Italy
European Laboratory for Non-linear Spectroscopy (LENS), Sesto Fiorentino, 50019, Italy

Dr. W. Sun, Dr. X. Zhang, Prof. Y. Li
National Key Laboratory of Science and Technology on Advanced Composites in Special Environments, Harbin Institute of Technology, Harbin, 150001, PR China
E-mail: yaoli@hit.edu.cn

Prof. C. Wang
Key Laboratory of Bio-Based Material Science and Technology of Ministry of Education
Material Science and Engineering, College Northeast Forestry University, Harbin, 150040, PR. China

Prof. J. Qiu
School of Energy Science and Engineering, Harbin Institute of Technology, Harbin, 150001, PR China

Prof. R. Yang
State Key Laboratory of Coal Combustion, School of Energy and Power Engineering,
Huazhong University of Science and Technology, Wuhan 430074, Hubei, PR China
E-mail: ronggui@hust.edu.cn

Keywords: Radiative sky cooling, Bioinspired surface, Thermal emissivity, Colorful radiative cooler, Refractive index matching

Coatings for passive radiative cooling applications must be highly reflecting in the solar spectrum, and thus can hardly support any coloration without losing their functionality. In this work, we report a colorful daytime radiative cooling surface based on structural coloration. A designed radiative cooler with a bioinspired array of truncated SiO_2 microcones is manufactured via a self-assembly method and reactive ion etching (RIE). Complemented with a silver reflector, the radiative cooler exhibits broadband iridescent coloration due to the scattering induced by the truncated microcone array while maintaining an average reflectance of 95% in the solar spectrum and a high thermal emissivity (ε) of 0.95, owing to the reduced impedance mismatch provided by the patterned surface at infrared wavelengths, reaching an estimated cooling power of ~143 W m^{-2} at an ambient temperature of 25 °C and a measured average temperature drop of 7.1 °C under direct sunlight. We attribute this strong cooling performance to its bio-inspired surface pattern, which promotes both the aesthetics and cooling capacity of the daytime radiative cooler.

1. Introduction

The energy needs for cooling are increasing at a fast pace worldwide, with buildings alone accounting for ~40% of the total global energy use and 28% of total CO_2 emission, according to statistics from the United States Department of Energy (DOE).[1] Similar needs can be found in the automotive sector, especially with the advent of electric vehicles whose batteries can be drained quickly by air-conditioning needs. Traditional cooling technologies suffer from several limitations: basically, they all rely on electricity, have high energy needs, and discharge waste heat into the surrounding environment which in turn contributes to global warming and the urban heat island effect.[2-4] For these reasons, the recent development of passive radiative sky cooling materials is attracting a growing interest due to its environmentally friendly nature and energy-free working principle.[5]

In recent years, hundreds of candidate materials have been proposed, offering a range of

passive cooling performances during daytime hours and even under direct sunlight. Two essential requirements for sub-ambient radiative cooling under direct sunlight are a high reflectivity above 90% in the solar spectral range (0.25-2.5 μm), and a strong, preferably selective emissivity in the atmospheric transparency window (8-13 μm).[6, 7] This demanding combination of optical properties is generally achieved through both the selection of specific materials with appropriate absorption bands and the micro and nano-engineering of coatings. These materials can be generally divided into four main categories, namely dielectric multilayer films,[8-12] organic-inorganic composite materials,[13-15] porous polymers,[16-20] and metamaterials.[21-25] Although many reported radiative coolers have achieved good cooling performance, these coatings are characterized by a broadband, high reflectivity over the whole solar spectrum, being thus limited to a white or mirror-like appearance at visible wavelengths. For certain applications, however, a colorful appearance may be more appealing, such as in the case of coatings and paints for the building and automotive sectors.[26] In addition, there still exist some issues with radiative cooling materials regarding fabrication complexity, poor stability to weathering agents, or the use of non-environmentally-friendly materials.

Previous attempts reported in the literature to obtain colorful radiative coolers relied on the addition of components with absorption peaks in the 300-800 nm range, such as dyes, nanoparticles, or the introduction of resonances for the selective enhancement of absorption.[27-33] For example, Son et al.[28] fabricated colorful radiative cooler using silica-embedded perovskite nanocrystals, resulting in white, green, and red-colored appearance depending on the color of nanocrystals. However, the color of quantum dots and dyes can easily change or fade due to oxidization or agglomeration, which leads to color instability. Alternatively, Zhu et al.[31] added a highly emissive structure on top of a colored nanowire array to cool it down. In cases like this one, however, the colorful appearance was obtained by introducing some absorption in the visible spectrum, which reduces the overall solar reflectance of the cooler and consequently deteriorates its cooling power. In a recent review paper by Zhou et al.[34] it was shown that vivid visual structural color can be produced by lossless structures. Structural colors have excellent durability, high saturation, bright colors, and do not fade with time or light exposure, holding great promise for improving the color stability of radiative coolers. Therefore, developing fabrication methods for radiative coolers exhibiting structural coloration and ultralow absorption in the visible spectrum is of high interest for several applications.

Inspired by the natural world, researchers have made significant progress toward the development of photonic materials with structural colors in recent years. For instance, the rainbow peacock spiders (*Maratus spp.*) present beautiful rainbow colors spanning the whole

visible spectrum owing to the optical diffraction induced by the prism grating on the surface of their abdominal scales. Such prism grating is composed of nano grooves with a typical feature size ranging from 500 to 800 nm, resulting in a bright iridescent coloration, [35, 36] due to the diffraction of the micro grating. Zhang et al.[37] demonstrated that a grating-like array of conical structures can suppress the total internal reflection and enhance the reflectivity of the radiative cooler in the UV-Vis-NIR region. Moreover, the fabricated micro grating enhances the infrared emissivity due to the reduced refractive index mismatch at its interface.[38-40] Therefore, a properly engineered micro grating could possibly play a threefold role by displaying a structural color, increasing the overall reflectance in the solar spectrum, and enhancing the IR emissivity of the structure.

Inspired by the rainbow peacock spider structure, we first used finite-difference time-domain (FDTD) numerical simulations to establish a database of simple microstructures and their average infrared emissivity (8-13 μm). One of the optimal results consists of a truncated microcone patterning of a SiO_2 surface, which can be conveniently fabricated via a combination of the self-assembly method and reactive ion etching (RIE). The radiative cooler displays indigo, blue, yellow, and pink colors as a result of angular-dependent diffraction. Its average thermal emissivity (ε) is also enhanced to 0.95 in the wavelength range of 8-13 μm, reaching an estimated cooling power of ~143 W m^{-2} and a corresponding temperature difference measured at noon of 7.1 °C below ambient temperature. The measured results are in excellent agreement with FDTD simulation results, which serve as a guide for the micro-nano structure design and confirm the origin of the proposed emissivity enhancement mechanism. By optimizing the photonic structure, we can increase the cooling efficiency of the radiative cooler while improving its aesthetics to encompass a wider range of application scenarios, providing a promising, durable, and industry-compatible method to produce colored passive radiative cooling coatings.

2. Results and discussion

To optimize a microstructure model with high infrared thermal emissivity over the 8-13 μm wavelength range, we performed FDTD simulations of an infinite periodic microcone array on a SiO_2 surface using the commercial FDTD Solutions software from Lumerical Solutions Canada.[41] The corresponding simulation schematic is shown in Figure S1a. The substrate model used in this simulation is a 2 μm thick SiO_2 with a side length of 4 μm and a 200 nm thick silver film serving as a reflector at the bottom. Cylindrical, conical, and truncated cone arrays with different structural dimensions are added on top of the substrate. **Figure 1**a-c shows three different microstructure models, with their corresponding simulated infrared thermal emissivity shown in Figure 1d-f. The numerical results show the good overall emissivity of the truncated microcone array compared to that of either cylindrical or conical elements. The infrared thermal emittance exhibits an increasing trend with the height of the scattering elements in the 8-13 μm wavelength range (Figure 1g). In particular, the thermal emittance is significantly enhanced around a wavelength of 9 μm when the truncated microcone height exceeds 0.8 μm, reaching a broadband (8-13 μm) emittance enhancement when the truncated microcones are about 2 μm tall. Such broadband emittance enhancement stems from the gradual refractive index gradient that the truncated microcones introduce, which helps reduce the impedance mismatch between silica and air in the atmospheric transparency window (8-13 μm).[39] For truncated cone array structures, the numerical simulations provide additional insight into the optimal periodicity and aspect ratio of the microcone array, with optimal emissivity found for a period of 1-2 μm and a length-diameter ratio larger than 1.5 (Figure 1h-i). These results provide useful information for the subsequent sample fabrication.

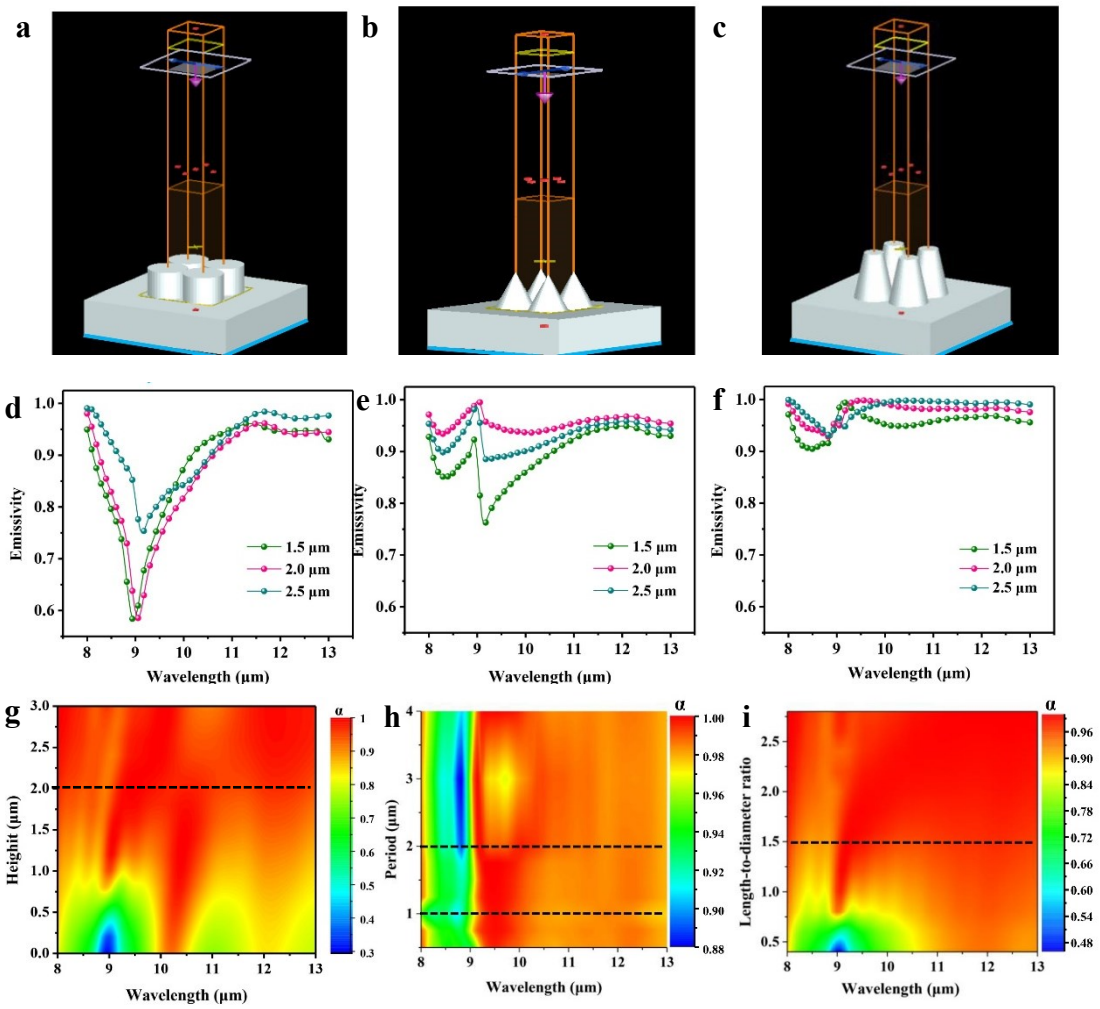

Figure 1. The layout of designed radiative coolers with microstructured silica: a) Cylindrical arrays (base diameter of 1 μm, height of 1.5 μm, 2 μm, and 2.5 μm); b) Conical arrays (base diameter of 1 μm, height of 1.5 μm, 2 μm, and 2.5 μm); c) Truncated microcone arrays (base diameter of 1 μm, top diameter of 0.5 μm, height of 1.5 μm, 2 μm, and 2.5 μm). d-f) The corresponding spectral emissivity curves over the atmospheric window (8-13 μm wavelengths). g) Optimization of the truncated cone height (H) in Figure S1a (from 0 to 3.4 μm) h) Optimization of the truncated cone period in Figure S1a (from 0.5 to 4 μm). i) Optimization of the length-diameter ratio of the truncated cone in Figure S1a (from 0.4 to 3). Dashed lines roughly represent the interval of stronger emissivity.

A schematic illustration of the fabrication process of the microstructured SiO_2 surface is shown in **Figure 2**a. Four different processing steps are involved in the fabrication of a micro cone array: evaporation, annealing, etching, and template removal. Scanning electron microscopy (SEM) images of the sample after each processing step are shown in Figure 2b and Figure S3a-

d. We start by depositing on the SiO_2 substrate an 80 nm thick Ag layer, which is then annealed at 550 °C for 2 h to spontaneously form Ag micro-islands with a diameter of about 0.2-1 μm, and a height between 0.2-0.5 μm. This self-assembly process is driven by the lower surface energy of the micro-island configuration on the SiO_2 surface. The micro-cone structures with a height of about 2 μm or more are then obtained by etching the SiO_2 layer using the Ag micro-islands as the etching masks. The dark patches at the top of the etched sample are the Ag residuals leftover (as shown in Figure S3c). After the removal of the Ag residuals, microstructures consisting of truncated microcones with an average height of about 2 μm are formed, and the average distance between the etched elements is about 1-2 μm (see Supplementary note 2 and Figure S3e-f for an analysis on the average areal density of truncated microcone array). We also studied the relationship between the etching time and etching depth (see Supplementary note 3 and Figure S4), showing that the tallest truncated microcone height (~2 μm) is obtained after 30 min of etching (three samples are obtained by etching times of 10, 20 and 30 minutes, which we name respectively Sample 1, Sample 2 and Sample 3). The surface of Sample 3 displays an iridescent coloration under different observation angles. To characterize the structural color change of Sample 3, we performed variable-angle reflection measurements from 10° to 60°. The results are reported in Figure 2c, showing a gradual redshift and intensity reduction of the main reflection peak, which moves from 380 to 650 nm. A corresponding coloration is observed on the surface of Sample 3, which was classified according to the Commission Internationale de L'Eclairage (CIE) 1931 chromaticity diagram and shown in Figure 2d, showing indigo, blue, green, yellow, and pink at 10°, 20°, 40°, 50°, and 60°, respectively. Photographs of the iridescent coloration are taken with a digital camera at different angles while keeping the illumination fixed, as shown in Figure 2e. The truncated microcone array (~2 μm) forms an efficient microstructured grating similar to that of the peacock spider, which is known for its bright display of structural colors ranging from bluish to yellow and pink hues [35, 36] An additional picture of the sample is shown in Figure S5, next to a simple silver-plated SiO_2 slide, showing its iridescent appearance in contrast with the flat spectral response of traditional coolers.

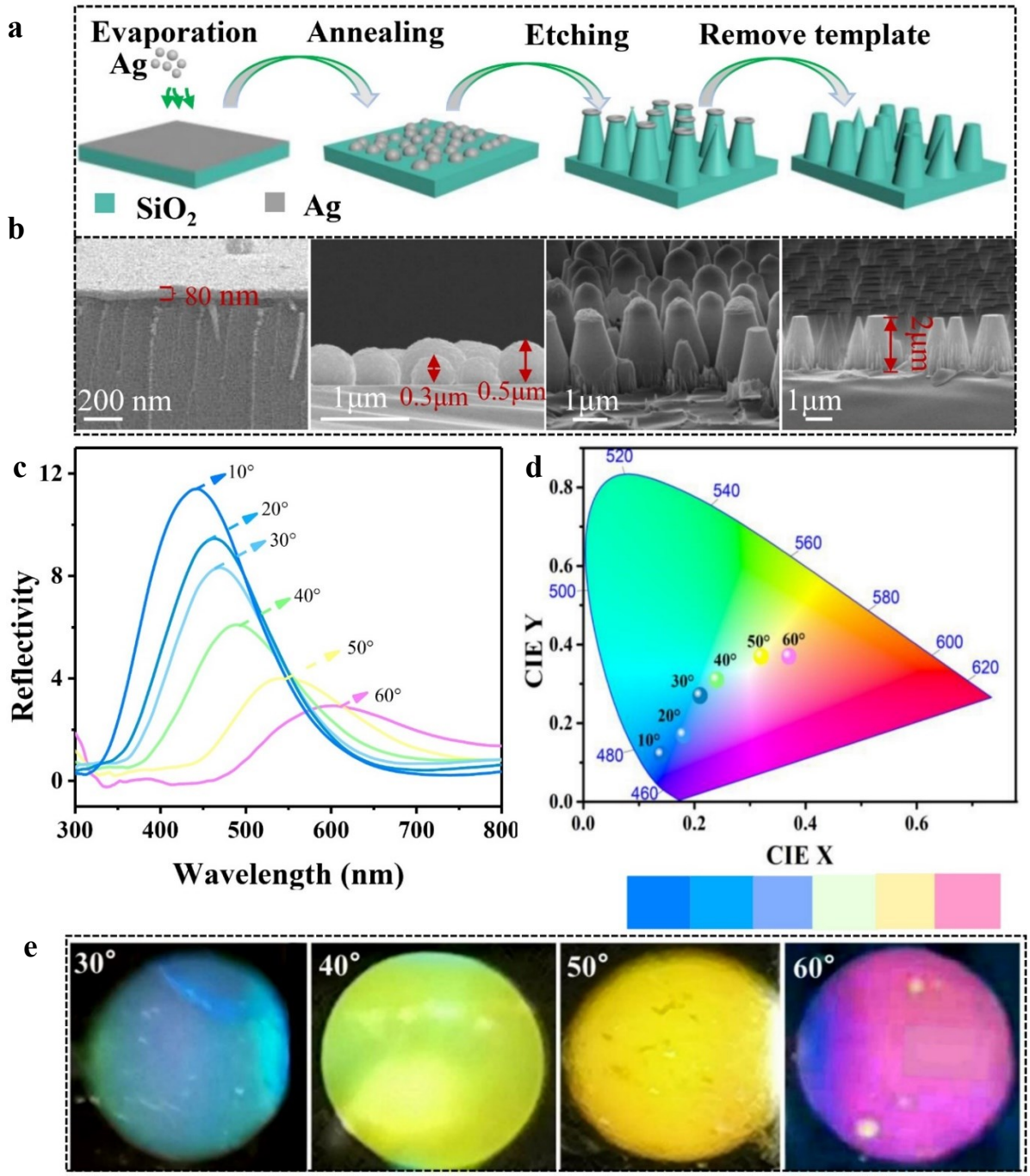

Figure 2. Fabrication process and structural color of the truncated microcone array on the surface of SiO_2: a) Fabrication process, b) The corresponding SEM images of the SiO_2 cross-section. c-e) Color effect characterization of Sample 3: c) The specular reflection spectrum of the surface of Sample 3 (from 10° to 60° at 10° intervals), d) Calculated CIE 1931 chromaticity diagrams. e) Optical images showing different colorations taken at different angles.

The reflectivity in the solar spectra (UV-Vis-NIR region, 0.25-2.5 μm wavelength) and emissivity in the thermal infrared region (2.5-25 μm wavelength) of different samples were characterized, and the corresponding results are shown in Figure S6. In the UV-Vis-NIR region,

the solar reflectance of Sample 1, Sample 2, and Sample 3 are almost the same and slightly above that of the silver-plated bulk SiO_2, while in the thermal infrared region, the sample with the highest truncated microcones (Sample 3) shows the best thermal infrared emissivity (ε=0.95) as predicted by numerical simulations. Therefore, in the following, we chose Sample 3 as the optimized sample for further study and the silver-plated, unpatterned SiO_2 as the benchmark sample for comparison, as shown in **Figure 3**a. Sample 3 exhibits a high average solar reflection, above 0.95 in the wavelengths ranging from 0.25 to 2.5 μm. The reflectivity enhancement observed for Sample 3 is due to the presence of the truncated microcone array. This particular surface pattern can effectively suppress total internal reflection,[37] while the corrugated air-glass interface further increases the reflectivity in the visible-NIR wavelength range by introducing an additional scattering contribution that is not present in the upatterned sample. Assuming negligible transmission through the Ag back-coating (200 nm), a solar absorptivity of 0.05 is estimated for the patterned samples. The infrared emissivity/absorptivity spectra of Sample 3 and silver-plated SiO_2 are shown in Figure 3b. The silver-plated SiO_2 has a relatively low average emissivity (~0.79) in the thermal infrared region (2.5-25 μm) (Figure 3b, blue curve), while Sample 3 shows a significantly higher value (~0.95) because the truncated microcone array of Sample 3 effectively suppresses the infrared reflection at the SiO_2-air interface occurring around 9 μm. An additional enhancement effect on the emissivity of Sample 3 may arise from the phononic resonances of the truncated microcone array.[23, 39] The emissivity and absorbance data of some relevant materials reported in the recent literature are summarized in Table S2, demonstrating that our microstructured SiO_2 surface compares favorably even against non-color-displaying samples in terms of these basic parameters. Among these, Wang et al.[16] reported a solar absorptivity of 0.05 and a remarkable infrared thermal emittance of 0.98 on a structural polymer coating, which however does not exhibit any coloration. In contrast, colored radiative coolers reported previously typically have a solar absorptivity value higher than 10%,[28, 34] which degrades the cooling performance when compared with a white radiative cooler. To estimate the theoretical limit of the cooling power of our samples, radiative cooling performance is theoretically evaluated using the AM1.5 solar spectrum and atmospheric absorption spectrum (the 1976 U.S. Standard), also considering variable non-radiative heat losses (see also Supplementary Note 1). The curves for the theoretical cooling power and temperature difference ΔT of Sample 3 assuming different values of h_{cc} are shown in Figure 3c, while that of Sample 1 and Sample 2 also are shown in Figure S7, where h_{cc} represents the non-radiative heat transfer coefficient relative to conduction and convection.[6] As expected by the previous spectral characterization, Sample 3 shows the highest net daytime radiative cooling

power (see also Table S3 for comparison with Samples 1 and 2). During a clear day, Sample 3 is expected to deliver 143.65 W m^{-2} at 25 ºC (Figure 3c), reaching an equilibrium temperature of 16.5 ºC, which is 8.5 °C lower than ambient temperature. Similarly, the temperature difference ΔT of Sample 1 and Sample 2 are 7.6 ºC and 8.1 ºC, respectively (Figure S7**)**, with an estimated net cooling power of 130.35 W m^{-2} and 138.17 W m^{-2}, respectively, under the same non-radiative heat losses of h_{cc} = 12 W m^{-2} K^{-1}. More importantly, in the ideal limit of no convection and conduction losses (h_{cc} = 0 W m^{-2} K^{-1}),[42, 43] the model returns a remarkable 32.9 ºC temperature drop in the daytime temperature for Sample 3, suggesting that the designed radiative cooler should retain a high cooling potential if additional IR-transparent insulation is applied to it.[44, 45] In comparison, an ideal sample (null absorption between 0.25 and 2.5 μm and unit emissivity between 2.5 and 25 μm, see Figure S8) shows an 11.6 ºC temperature drop, while the bulk SiO_2 cannot be cooled as its curve value is negative at equilibrium. On the other hand, the silver-coated SiO_2 sample and Sample 3 show a 5.7 ºC and 8.5 ºC temperature drop, respectively. The cooling performance of SiO_2 after silver deposition is mainly due to the high average solar reflectance of this sample, while the cooling performance of Sample 3 is better than the other samples due to its optimized IR emissivity and solar reflectance (Figure 3a and Figure 3b).

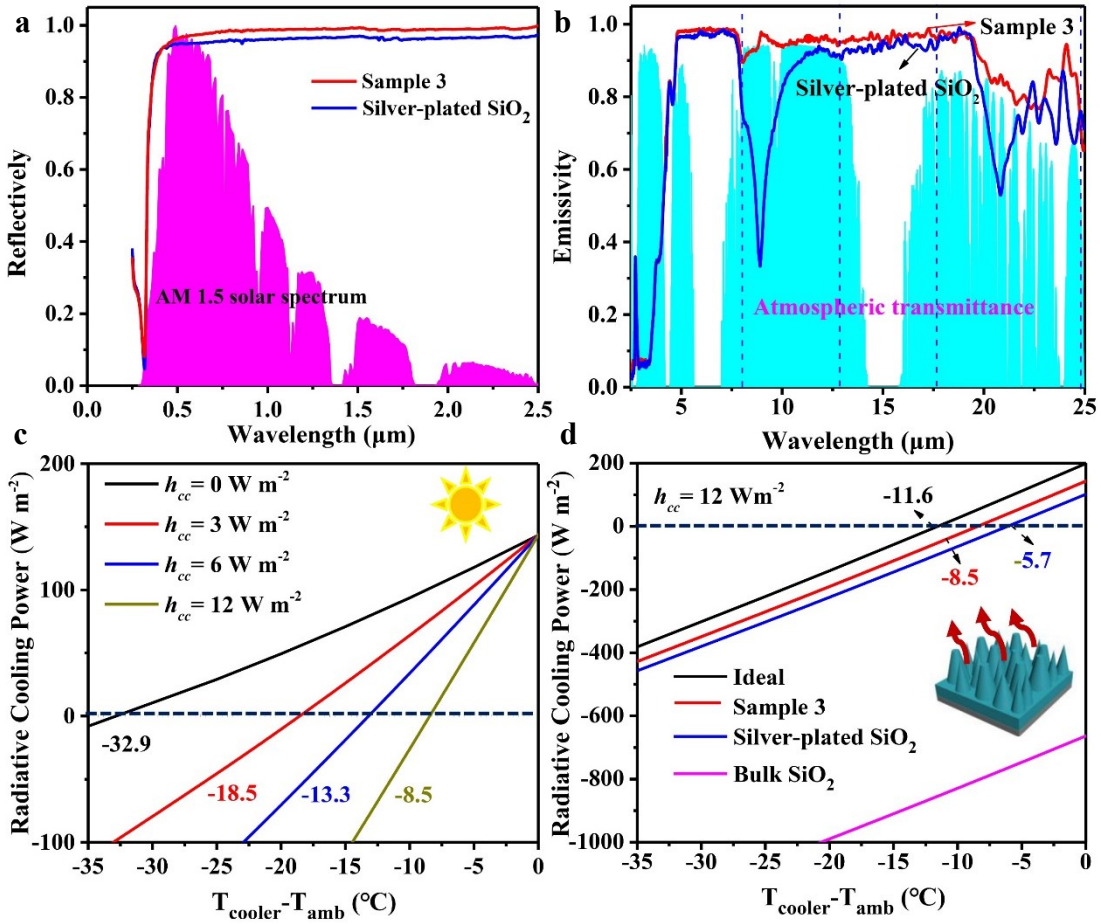

Figure 3. Cooling performance of the different samples. a) Measured reflectivity over the solar spectrum (0.25-2.5 μm), the AM 1.5 solar spectrum is also shown for reference. b) Measured emissivity/absorptivity in the mid-to-long infrared wavelengths from 2.5 to 25 μm, together with the atmospheric transmittance. c) Theoretical cooling flux of Sample 3 as a function of temperature difference ΔT, T_a = 25 ºC (h_{cc} is 0 W m^{-2} K^{-1}, 3 W m^{-2} K^{-1}, 6 W m^{-2} K^{-1}, 12 W m^{-2} K^{-1}). d) Theoretical cooling flux of different samples as a function of temperature difference ΔT under the same conditions (h_{cc} = 12 W m^{-2} K^{-1}).

Field tests were conducted to investigate the cooling performance of designed different coolers (Sample 1, Sample 2, Sample 3, Silver-plated SiO_2) on the same day July 24 2021 at the Harbin Institute of Technology in Harbin City, China. An outdoor temperature measurement setup was implemented on the roof of the laboratory building, and the schematic diagram of the temperature measurement device is shown in **Figure 4**a. The outside test box (transparent acrylic bracket) is supported by three vertical glass rods and covered with a layer of polyethylene film forming a sealed pocket of air within the test chamber (Figure S9). The polyethylene film is used as a transparent windshield to reduce non-radiative convection and conduction heat losses. The radiative cooler has a thermocouple installed on the back surface,

monitoring the temperature under the sample and in the test chamber. IR thermography measurements in Figure 4b further confirm the cooling performance of Sample 3. After reaching thermal equilibrium under direct sunlight, Sample 3 reaches a temperature of 26.1 ºC, which is about 2.7 ºC lower than that of an unpatterned silver-plated SiO_2. The observed temperature drop for the optimized coating (Sample 3) is reported in Figure 4c, showing an average daytime temperature difference of 7.1 °C with its environment during the measurement period (maximum difference registered of 8.9 °C). T_{amb} and T_{cooler} rose and fell in sync with the rising and setting of the sun during the daytime test, and the temperature drop ΔT is given in Figure 4d by subtracting T_{cooler} from T_{amb}. Similar measurement results are reported in Figure S10 for the other two samples, showing average temperature drops of 4.6 °C and 6.5 °C, respectively. In comparison, the maximum and average values recorded for the silver-plated SiO_2 are 6.2 ºC and 4.5 ºC. An additional open ambient temperature test was conducted in the mild environment conditions of Suzhou (February 26, 2022), which again showed temperature drops between 5 and 7 °C around noontime (Figure S11).

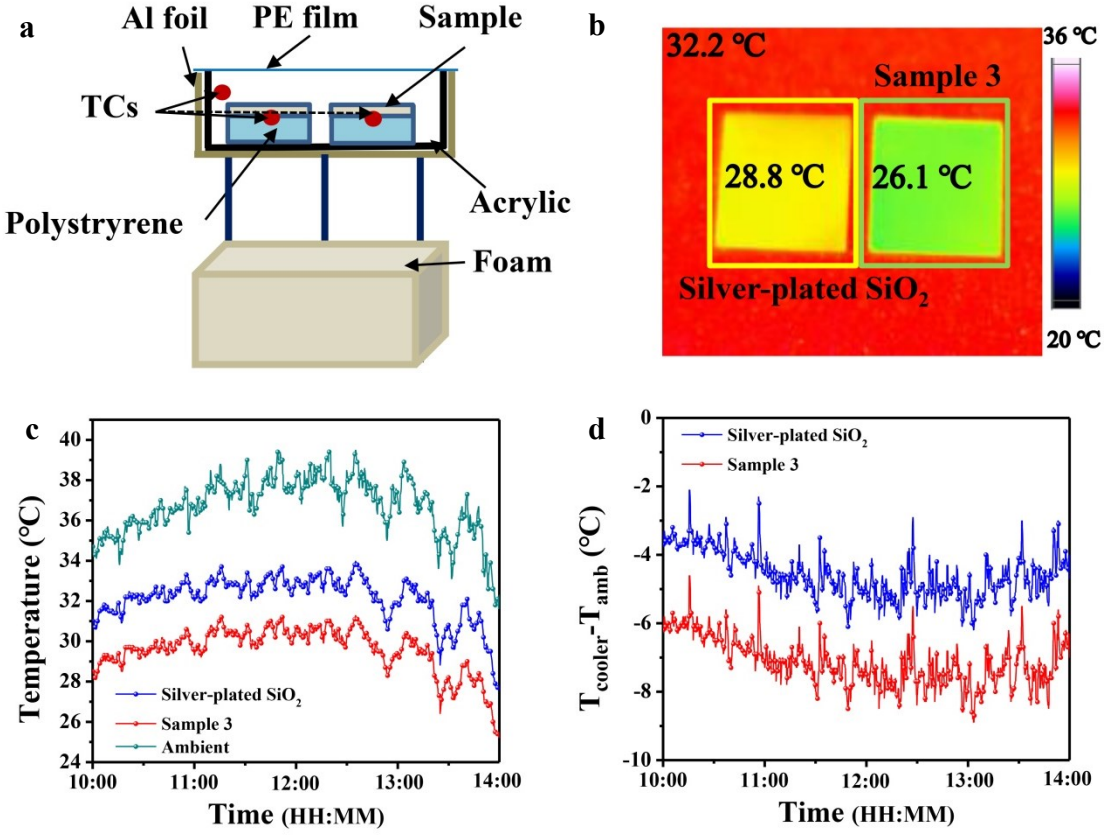

Figure. 4. The cooling performance of the different samples. a) Schematic of the outdoor measurement setup. b) IR thermography comparing Sample 3 and silver-plated SiO_2, measured without the windshield. c) Measured temperature change of Sample 3 and silver-plated SiO_2 under clear sky conditions. d) The corresponding temperature drop ΔT.

We compared the measured results and FDTD simulation results of thermal infrared emission over the atmospheric window band (8-13 μm). Based on the morphological analysis of the fabricated structure, a more realistic model was also considered, mixing both conical and truncated conical elements. The resulting emissivity curves are shown in Figure S12, showing that the non-uniform arrays exhibit intermediate emissivity values between the two cases, resulting in a smoother and more uniform emissivity across the transparency window. **Figure 5**a further shows the angular emissivity over the 8-13 μm wavelengths between 0° and 70°. For the bulk SiO_2, the value drops rapidly when the angle is larger than 45°, while the optimized microstructured SiO_2 surface exhibits an average emissivity above or close to 0.9 up to 60°. Figures 5b shows the emissivity curves of the bulk SiO_2 and microstructured SiO_2. The emittance of bulk SiO_2 at a wavelength of 9 μm is about 0.3, while the microstructured SiO_2 can achieve an emittance above 0.9, in good agreement with the experimental results. This suggests that the truncated microcone array has significantly reduced the impedance mismatch between air and SiO_2 surface.[46] The microcone pattern has also a strong impact on the angular emissivity of the radiative cooler, which becomes both larger and broader with respect to the unpatterned case. A similar angular broadening of the emissivity distribution was also recently observed in other structures with micrometer-sized surface features,[16, 40] and could be beneficial to the overall cooling performance of samples having broad and unobstructed sky access. The observed emissivity enhancement, on the other hand, can be explained by the reduction of the large impedance mismatch that is characteristic of silica around 9 μm, due to its bulk phonon-polariton resonances. The fabricated mixture of conical and truncated conical elements effectively suppresses the material reflectance, as already reported by previous works involving similar patterns of SiO_2 elements.[39, 40, 47]

To explore the emissivity enhancement mechanism provided by the non-uniform arrays the electric field distributions of microstructured SiO_2 and bulk SiO_2 were examined at 8.9 μm, 9.1 μm, and 9.3 μm wavelengths. In Figure 5c and Figure S13 (a-h). As shown in Figure S13(a-d), the electric field distribution of the simulated bulk SiO_2 at different wavelengths shows a demarcation at the sample interface due to the strong reflection which is observed in this wavelength range (Figure 5b). On the other hand, in the microstructured case, a field enhancement localized around the truncated microcones exhibiting shows a strong amplitude variation of 1.3 (Figure 5c), much larger than the amplitude variation of 0.3 observed for bulk SiO_2. This implies that the microstructured arrays can overcome impedance mismatch and enhance the spectral absorption of SiO_2 in these wavelengths.[48] These simulation results

suggest that the microstructured pattern is conducive to obtaining a stronger coupling with the structure and a smoother index matching with the environment, thus leading to a higher extinction in the thermal infrared wavelength range.

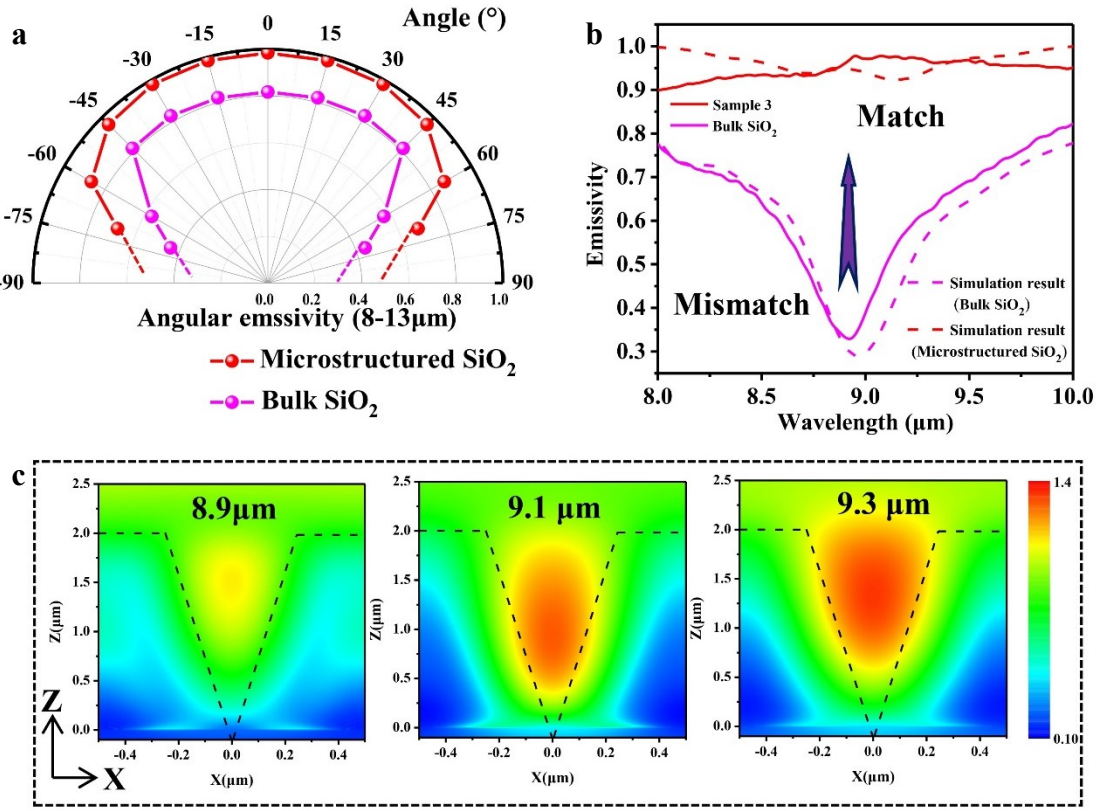

Figure 5. FDTD simulation results for the bulk SiO_2 and microstructured SiO_2 (8-13 μm). a) Simulated average angular emissivity. b) Emissivity of simulated and prepared samples (bulk SiO_2 and microstructured SiO_2) around the 9 μm resonance wavelength. c) The simulated Y-component of the electric field in the X-Z plane around the 9 μm resonance (8.9 μm, 9.1 μm, and 9.3 μm).

3. Conclusion

In summary, we have designed and developed an iridescent radiative cooler based on a bioinspired truncated microcone array of SiO_2. The colorful radiative cooler (Sample 3) exhibits a continuous change from red to blue under different incident light angles while achieving a solar reflectance of 95% and an average thermal emissivity (ε) of 0.95 over the atmospheric window owing to its engineered microcone structure. This designed colorful radiative cooler exhibited an average temperature difference of 7.1 ºC in late July in Harbin City with respect to ambient temperature, for an estimated net cooling power of ~140 W m^{-2}. FDTD simulations are in good agreement with the thermal infrared emissivity enhancement induced by the 2 μm-

tall truncated microcone array, shedding light on the underlying enhancement mechanism and providing guidance for the design of microstructured SiO_2 emitters. Most remarkably, our designed cooler exhibits a distinct iridescent coloration without reducing its high solar reflectance, thus allowing it to preserve its sub-ambient cooling performance while offering an interesting opportunity for aesthetics.

4. Experimental Section

Materials: Quartz substrates (SiO_2) 20×40×1 mm^3 in size were purchased from Aladdin. All other chemicals including Nitric acid (HNO_3), silver (Ag), ethanol (C_2H_5OH), and acetone (CH_3COCH_3) were purchased as analytical grade reagents from Tianjin Tianli Chemical Reagents Ltd. All experimental gases including argon (Ar, 99.99%), nitrogen (N_2, 99.99%) and trifluoromethane (CHF_3, 99.99%) were purchased from Harbin Liming Gas Co., Ltd.

Fabrication of self-assembled silver island template and radiative cooling device: The preparation process of Ag islands was divided into two main parts: vapor deposition and annealing. Before deposition, the quartz substrate was washed by sonication in deionized water, acetone, and ethanol for 15 min each. The washed quartz plate was then transferred into the deposition chamber. The chamber was pumped down to 5×10^{-3} Pa before deposition, and the distance from the sample sheet to the targets was set to about 30 cm. The thickness of the final deposited Ag film was about 80 nm. The Ag film was transferred to a tube furnace for the annealing treatment. An annealing temperature of 550 °C was reached with a heating rate of 5 °C min^{-1} and maintained for 2 h. The entire annealing process was performed under high purity Ar (99.99%) flow. The subsequent dry etching process was carried out using an NRE-4000 system (Nano-Master, Inc, USA). The 50 Watt power supply was assigned for the platen bias (RF1), while the 150 Watt power supply was connected to the Inductive Coupled Plasma Emission Spectrometer (ICP) source on the top (RF2). The parameters used for the etching processes were summarized in Table S1 for 3 different etching times. In the reactive ion etching process, the flow rates of trifluoromethane (CHF_3) and argon (Ar) were set to 20 and 8 sccm, respectively, and the pressure of the etching chamber was calibrated to 50 mtorr. The etching time was 10 to 40 min with a gradient rise, starting as soon as the etching chamber reaches a pressure below 4×10^{-5} mtorr. Next, the sample was washed for 30 min in a 10% nitric acid bath to get the microstructured sample (no residual silver). A 200 nm Ag layer was deposited again on the backside of the washed sample to serve as a reflective substrate. Finally, to protect the

silver layer, an 80 nm silicon oxide protective layer is vaporized on the surface of the silver layer. We estimate a cost for the resulting structure of approximately \$0.20/cm^2, as detailed in Supplementary Note 5.

Measurements: The outdoor temperature measurement was carried out at Harbin Institute of Technology, Harbin City (N 45° 44' 49", E 126° 37' 50", Altitude 128 m) in clear weather on 24 July 2021 (average humidity 50%). The morphologies of all sample surfaces and sections were observed by Scanning Electron Microscopy (SEM) (SIGMA 300, ZEISS, Germany). The solar spectral reflectance was determined by a UV-Vis-NIR spectrophotometer (Lambda-950, Perkin Elmer, US) with a wavelength range of 0.25 to 2.5 μm. The infrared spectral reflectance of the samples in the wavelength from 2.5 to 25 μm was measured by an FT-IR spectrometer with an A562 integrating sphere. Thermal images of the samples were obtained using an IR thermal imager (Tix660, Fluke) with a spectral range of 7.5-14 μm.

Supporting Information

Supporting Information is available from the Wiley Online Library or the author.

Acknowledgments

We thank the National Natural Science Foundation of China (No. 51702068, 52072096, 51572058, 51902073, 52076062), the China Postdoctoral Science Foundation Funded Project (2019M661273), and the Fundamental Research Funds for the Central Universities (HIT. NSRIF. 2020019, HIT OCEF. 2021004, FRFCU5710090220), Heilongjiang Postdoctoral Fund (LBH-Z15078, LBH-Z16080).

Conflicts of interest

There are no conflicts to declare.

Author Contributions

J. Zhao and H. Xu conceived the idea. Y. Li provides the resources and funding acquisition. Z. Ding initiated the project and wrote the first draft. L. Pan, W. Sun, and J. Qiu provided the simulated data obtained by FDTD and MATLAB. X. Li set up the experimental equipment. R. Yang, L. Pattelli, C. Wang, Y. Song, and X. Zhang revised the manuscript. All authors discussed the results and contributed to the writing.

Received: ((will be filled in by the editorial staff))
Revised: ((will be filled in by the editorial staff))
Published online: ((will be filled in by the editorial staff))

References

[1] N. Wang, P. E. Phelan, C. Harris, J. Langevin, B. Nelson, K. Sawyer, *Renew. Sust. Energ. Rev.* **2018**, *82*, 976.

[2] B. I. Cook, J. E. Smerdon, R. Seager, S. Coats, *Clim. Dynam.* **2014**, *43*, 2607.

[3] F. Ascione, *Sol. Energy* **2017**, *154*, 34.

[4] S. C. Sherwood, M. J. Webb, J. D. Annan, K. C. Armour, P. M. Forster, J. C. Hargreaves, G. Hegerl, S. A. Klein, K. D. Marvel, E. J. Rohling, M. Watanabe, T. Andrews, P. Braconnot, C.S. Bretherton, G. L. Foster, Z. Hausfather, A. S. Heydt, R. Knutti, T. Mauritsen, J. R. Norris, C. Proistosescu, M. Rugenstein, G. A. Schmidt, K. B. Tokarska, M. D. Zelinka, *Rev. Geophys.* **2020**, *58*, 4.

[5] X. Yin, R. Yang, G. Tan, S. Fan, *Science* **2020**, *370*, 786.

[6] D. Zhao, A. Aili, Y. Zhai, S. Xu, G. Tan, X. Yin, R. Yang, *Appl. Phys. Rev.* **2019**, *6*, 021306.

[7] R. Family, M. P. Mengüç, *Procedia Environmental Sciences* **2017**, *38*, 752.

[8] Y. Shi, W. Li, A. Raman, S. Fan, *ACS Photonics* **2017**, *5*, 684.

[9] D. Chae, M. Kim, P. H. Jung, S. Son, J. Seo, Y. Liu, B. J. Lee, H. Lee, *ACS Appl. Mater. Interfaces* **2020**, *12*, 8073.

[10] H. Ma, K. Yao, S. Dou, M. Xiao, M. Dai, L. Wang, H. Zhao, J. Zhao, Y. Li, Y. Zhan, *Sol. Energ. Mat. Sol. C.* **2020**, *212*, 110584.

[11] A. P. Raman, M. A. Anoma, L. Zhu, E. Rephaeli, S. Fan, *Nature* **2014**, *515*, 540.

[12] Y. Dai, Z. Zhang, C. Ma, *Opt. Commun.* **2020**, *475*, 126231.

[13] S. Zhong, L. Yi, J. Zhang, T. Xu, L. Xu, X. Zhang, T. Zuo, Y. Cai, *Chem. Eng. J.* **2021**, *407*, 127104.

[14] D. Lee, M. Go, S. Son, M. Kim, T. Badloe, H. Lee, J. K. Kim, J. Rho, *Nano Energy* **2021**, *79*, 105426.

[15] L. Zhou, H. Song, J. Liang, M. Singer, M. Zhou, E. Stegenburgs, N. Zhang, C. Xu, T. Ng, Z. Yu, B. Ooi, Q. Gan, *Nat. Sustain.* **2019**, *2*, 718.

[16] T. Wang, Y. Wu, L. Shi, X. Hu, M. Chen, L. Wu, *Nat. Commun.* **2021**, *12*, 365.

[17] S. Son, Y. Liu, D. Chae, H. Lee, *ACS Appl. Mater. Interfaces* **2020**, *12*, 57832.

[18] J. Mandal, Y. Fu, A. C. Overvig, M. Jia, K. Sun, N. N. Shi, H. Zhou, X. Xiao, Y. Yang, N. Yu, *Science* **2018**, *362*, 315.

[19] H. Zhao, Q. Sun, J. Zhou, X. Deng, J. Cui, *Adv. Mater.* **2020**, *32*, 2000870.

[20] B. Xiang, R. Zhang, Y. Luo, S. Zhang, L. Xu, H. Min, S. Tang, X. Meng, *Nano Energy* **2021**, *81*, 105600.

[21] Y. Lu, Z. Chen, L. Ai, X. Zhang, J. Zhang, J. Li, W. Wang, R. Tan, N. Dai, W. Song, *Sol. RRL* **2017**, *1*, 1700084.

[22] D. Zhao, A. Aili, Y. Zhai, J. Lu, D. Kidd, G. Tan, X. Yin, R. Yang, *Joule* **2019**, *3*, 111.

[23] Y. Zhai, Y. Ma, S. N. David, D. Zhao, R. Lou, G. Tan, R. Yang, X. Yin, *Science* **2017**, *355*, 1062.

[24] N.N. Shi, C. C. Tsai, F. Camino, G. D. Bernard, N. Yu, R. Wehner, *Science* **2015**, *349*, 298.

[25] C. Zou, G. Ren, M. M. Hossain, S. Nirantar, W. Withayachumnankul, T. Ahmed, M. Bhaskaran, S. Sriram, M. Gu, C. Fumeaux, *Adv. Opt. Mater.* **2017**, *5*, 1700460.

[26] W. Li, Y. Shi, Z. Chen, S. Fan, *Nat. Commun.* **2018**, *9*, 4240.

[27] H. H. Kim, E. Im, S. Lee, *Langmuir* **2020**, *36*, 6589.

[28] S. Son, S. Jeon, D. Chae, S. Y. Lee, Y. Liu, H. Lim, S. J. Oh, H. Lee, *Nano Energy* **2021**, *79*, 105461.

[29] G. B. Smith, A. Gentle, P. D. Swift, A. Earp, N. Mronga0, *Sol. Energy Mater. Sol. C.* **2003**, *79*, 179.

[30] C. Sheng, Y. An, J. Du, X. Li, *ACS Photonics* **2019**, *6*, 2545.

[31] L. Zhu, A. Raman, S. Fan, *Appl. Phys. Lett.* **2013**, *103*, 223902.

[32] G. J. Lee, Y. J. Kim, H. M. Kim, Y. J. Yoo, Y. M. Song, *Adv. Optical Mater.* **2018**, *6*, 1800707.

[33] R. A. Yalçın, E. Blandre, K. Joulain, J. Drévillon, *ACS Photonics* **2020**, *7*, 1312.

[34] L. Zhou, J. Rada, H. Song, B. Ooi, Z. Yu, Q. Gan, *J. Photon. Energy* **2021**, *11*, 042107.

[35] B. K. Hsiung, R. H. Siddique, D. G. Stavenga, J. C. Otto, M. C. Allen, Y. Liu, Y. F. Lu, D. D. Deheyn, M. D. Shawkey, T. A. Blackledge, *Nat. Commun.* **2017**, *8*, 2278.

[36] D. E. McCoy, V. E. McCoy, N. K. Mandsberg, A. V. Shneidman, J. Aizenberg, R. O. Prum, D. Haig, *Proc. Biol. Sci.* **2019**, *286*, 20190589.

[37] H. Zhang, K. C. S. Ly, X. Liu, Z. Chen, M. Yan, Z. Wu, X. Wang, Y. Zheng, H. Zhou, T. Fan, *Proc. Natl. Acad. Sci. U. S. A.* **2020**, *117*, 14657.

[38] M. L. Brongersma, Y. Cui, S. Fan, *Nat. Mater.* **2014**, *13*, 451.

[39] L. Zhu, A. Raman, K. X. Wang, M. A. Anoma, S. Fan, *Optica* **2014**, *1*, 32.

[40] L. Zhu, A. P. Raman, S. Fan, *Proc. Natl. Acad. Sci. U. S. A.* **2015**, *112*, 12282.

[41] J. Vaillant, A. Crocherie, F. Hirigoyen, A. Cadien, J. Pond, *Opt. Express* **2007**, *15,* 5494.

[42] J. Zhang, J. Yuan, J. Liu, Z. Zhou, J. Sui, J. Xing, J. Zuo, *Renew. Sust. Energ. Rev.* **2021**,

143, 110959.

[43] M. Yang, W. Zou, J. Guo, Z. Qian, H. Luo, S. Yang, N. Zhao, L. Pattelli, J. Xu, D. S. Wiersma, *ACS Appl. Mater. Interfaces* **2020**, *12*, 25286.

[44] M. Yang, W. Zou, J. Guo, Z. Qian, H. Luo, S. Yang, N. Zhao, L. Pattelli, J. Xu, D. S. Wiersma, *ACS Appl. Mater. Interfaces* **2020**, *12*, 25286.

[45] A. Leroy, B. Bhatia, J. Sircar, E.N. Wang, *International Journal of Heat and Mass Transfer* **2022**, *184*, 122307.

[46] G. L. Whitworth, J. Jaramillo-Fernandez, J. A. Pariente, P. D. Garcia, A. Blanco, C. Lopez, C. M. Sotomayor-Torres, *Opt. Express* **2021**, *29*, 16857.

[47] J. Jaramillo-Fernandez, L. Whitworth, J. Pariente, A. Blanco, P. D. Garcia, C. Lopez, C.M. Sotomayor-Torres, *Small* **2019**, *15*, 1905290

[48] Z.Wang, H. Ding, D. Liu, C. Xu, B. Li, S. Niu, L. Ren, *ACS Appl. Mater. Interfaces* **2021**, *13*, 23103.